To: APEX GROUP
From: Anter El-Azab (anter@seas.ucla.edu)
Re: NWL Limits in Current Concepts

Memo No. AAE_032798_1
Dat e: March 27, 1998

Dear Colleagues,

In the last two APEX meetings, the contents of this document --on the limitation of current concepts in handling high power density-- were presented. Essentially, NWL limits calculations for the three reduced-activation materials (Steel and Vanadium alloys and SiC-SiC composites) are discussed, along with the underlying calculation assumptions. I tried here to summarize the materials data that was used in the calculations. This data are based on the previous two presentations and materials data summaries prepared by Dr. Zinkle and other ORNL Colleagues. Relevant properties and NWL limits for three refractory materials --Nb-1Zr, T111 and TZM-- are also added, as was suggested to me by Professor M. Abdou and Dr. Zinkle.

Best Regards,

Anter

LIMITATION OF CURRENT MAGNETIC FUSION DEVICE CONCEPTS IN HANDLING HIGH POWER DENSITY

I. INTRODUCTION

Materials limitations represent the natural boundaries for engineering design windows. A component made of a specific material must have operating parameters within the limits dictated by the response of the material being used. In fusion devices, the service conditions, characterized by high temperature, intense irradiation fields, high stresses, electromagnetic fields, hot chemistry, etc., lead to 1) development of undesired microstructures; 2) initiation and evolution of bulk damage; and, in turn, 3) significant changes in the material thermomechanical and physical properties. Such effects result in changes of the natural design windows dictated by the materials limits.

The fusion program is currently assessing Blanket/First Wall (B/FW) concepts which are capable of handling Neutron Wall Loads (NWL) on the order of $7MW/m^2$ or higher, and surface heat loads on the order of $2MW/m^2$. These concepts are termed "High Power Density Concepts" (HPDCs). The term high power density, in the present context, implies high surface heat flux and high neutron wall loading. This of course implies (overall) higher ratio of reactor power to the power recovery surface area/volume. The magnitude $2MW/m^2$ of the surface heat load comes along from the assumption that a fraction of ~80% or higher of the alpha-power is radiated by the plasma to the first wall, thus relieving the need for divertors with high surface load capability. Recent experiments from the JET program [1] showed that controlling the impurities in the plasma may indeed result radiating most of the alpha power to the first wall more or less uniformly. Plasma radiation to the FW consists of Bremsstrahlung and line radiation. While the detailed nature of the line radiation is strongly dependent on the plasma composition, the majority of radiation which is in the form of Bremsstrahlung is considered to carry the alpha-power out of the plasma. If this is the case, the surface heat load scales linearly with the neutron wall load to a reasonable degree of accuracy.

In the context of searching for and evolving the HPDCs, it is important to assess the wall loading limits for conventional solid first walls made of Ferritic Steel, V-Cr-Ti Alloys, and SiC-SiC composites. These three materials are currently under development/feasibility investigation as prospective fusion structural materials with low activation characteristics. Assessment of the wall load limits for these three materials is conducted here to make a judgment on whether conventional First Wall (FW) made out of these materials can withstand high surface heat loads. A conventional FW/B design may be warrant further evolution if these one or more of these material choices prove not to limit the NWL to below $5MW/m^2$.

The search of HPDCs is not restricted to concepts based on the three candidate materials mentioned above. Rather, other high-temperature resistant materials, refractory alloys in particular, which do not satisfy the low activation requirements are also considered as potential structural materials that enable reaching the attractiveness goal of handling high power densities. In this context, alloys of Niobium (e.g., Nb-1Zr), Tantalum (e.g., T111) and Molybdenum (e.g., TZM) are evaluated.

Does high power density imply high operating temperatures? In a sense, the answer is yes. If surface heat removal from the first wall relies on heat conduction through the wall to a first wall coolant, a specific temperature difference across the first wall must be established in order to conduct the surface heat. The maximum wall temperature is then determined by the structure-coolant interface temperature. Two material limits appear: allowable maximum temperature and allowable maximum stress. These two material limits are the key limits to be dealt with in assessing the wall load limits in the present study.

II. MATERIALS PROPERTIES AND STRESS AND TEMPERATURE LIMITS

II.1 Reduced-Activation Materials

The stress limits for the three materials (Ferritic Steel, V-Cr-Ti and SiC-SiC composites) are briefly discussed here. Only the unirradiated materials data are shown, on the basis that the beginning of life limits are being assessed.

A) FERRITIC STEEL

The ultimate tensile strength for several heats of Fe-(8-9)%Cr reduced activation steels has been measured by several researchers. Fig. 1 summarizes some of the ultimate tensile strength (UTS) data obtained in tensile tests on F82H (Fe-8%Cr-2%WVTa) and other heats [2-5]. The least squares fitted equation for the ultimate tensile strength over the temperature range of 20-700•C is

$$\sigma_{UTS}(MPa)= 682.8 -1.1617*T +0.005472*T^2 -1.1166e-05*T^3 +6.2357e-09*T^4$$

where the temperature (T) is in •C. The correlation coefficient for the plotted data using this equation is R=0.8955.

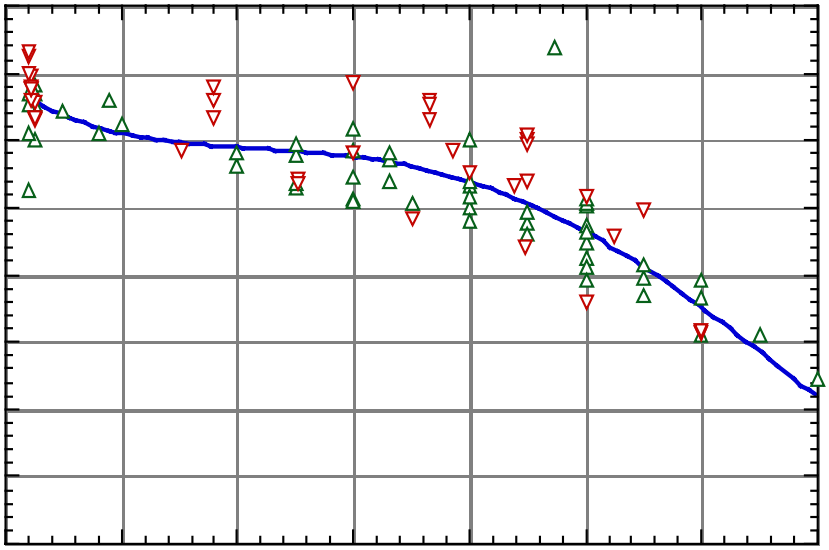

Fig. 1: Ultimate tensile strength of unirradiated 8-9%Cr steels [2-5].

Fig. 2 summarizes the yield strength data obtained on several heats of Fe-(8-9)%Cr reduced activation steels. The least squares fitted equation for the yield strength over the temperature range of 20-700•C is

$$\sigma_Y(\text{MPa}) = 531.37 - 0.38794*T + 0.001482*T^2 - 2.3965e\text{-}06*T^3 - 1.4506e\text{-}10*T^4$$

where the temperature (T) is in •C. The correlation coefficient for the plotted data using this equation is R=0.8835.

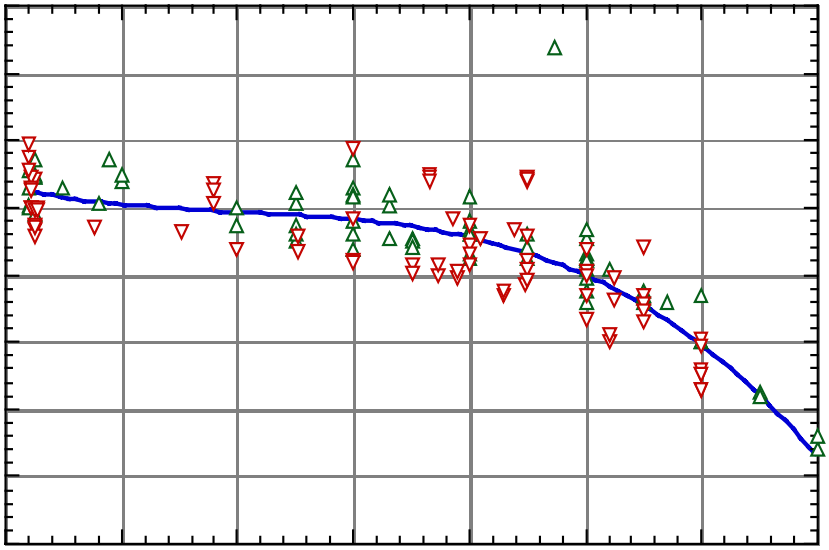

Fig. 2: Yield strength of unirradiated 8-9%Cr steels [2-5].

The elastic constants for F82H (8Cr-2WVTa) have been measured between 20 and 700•C [4]. The Young's modulus varies approximately linearly from 217 to 193 GPa as the temperature is increased from 20 to 450C, and then linearly decreases to 160 GPa at 700•C. The shear modulus similarly decreases from 84 to 75 GPa, and then to 60.5 GPa as the temperature is increased from 20 to 450•C and then to 700•C. The Poisson's ratio is constant up to 500•C with a value of 0.29, and then slowly increases to 0.31 at 700•C. The change in the temperature dependence of the elastic constants at 450-500•C was attributed to annealing effects on the martensitic structure at the higher temperatures [3].

The thermophysical properties for several different heats of F82H (8Cr-2WVTa) have been measured from room temperature to 700•C [2,4]. The instantaneous coefficient of thermal expansion (α_{th}) varied from 10.4 ppm/•C at room temperature to 12.4 ppm/•C at 700•C. The thermal conductivity at 20-800•C was determined from thermal diffusivity measurements using laser flash techniques. The thermal conductivity for two heats of F82H was nearly independent of temperature in this temperature range, with an average value of 33 W/m-K between 20 and 700•C.

The maximum operating temperature limit for 8-9%Cr reduced activation ferritic/martensitic steels is ~550•C, due to thermal creep considerations. Somewhat higher temperatures could be tolerated for components exposed to low mechanical stresses. Additional work on irradiated specimens is needed before the minimum operating temperature limit can be established. The reference minimum operating temperature limit will be controlled by radiation hardening, which

causes loss of ductility and an increase in the ductile to brittle transition temperature. According to the available irradiation data, the DBTT of 8-9%Cr steels remains near or below room temperature following neutron irradiation at temperatures between 200 and 550•C [3,8,11-13]. There is some limited evidence that fusion-relevant helium generation rates may cause a further increase in the DBTT beyond that attributable to matrix hardening (defect cluster) effects [7,12]. Further work is needed to determine the effect of helium on fracture properties. For the purposes of the APEX design study, the proposed reference minimum operating temperature for 8-9%Cr steels is 250•C.

B) VANADIUM ALLOYS

The ultimate tensile strength for the BL47 (30 kg) [14] and Teledyne Wah Chang #832665 (500 kg) [14-16] heats of V-4Cr-4Ti has been measured by several researchers. Fig. 3 summarizes ultimate tensile strength (UTS) data obtained in tensile tests at strain rates near $1x10^{-3}$ s^{-1} on annealed (1000-1100•C for 1 to 2 h) specimens in the longitudinal orientation. The data in refs. [14,15] were obtained on "type SS3" miniature sheet tensile specimens with gage dimensions of 0.76 x 1.52 x 7.6 mm, whereas the data in ref. [16] were obtained on round tensile specimens with gage dimensions of 4 mm diam x 20 mm. Good agreement was obtained for both types of specimen geometries over the investigated temperature range. The least squares fitted equation for the ultimate tensile strength over the temperature range of 20-700•C is

$$\sigma_{UTS}(MPa)= 445.72 -0.80616*T +0.002211*T^2 -1.7943e-06*T^3 +1.8176e-10*T^4$$

where the temperature (T) is in •C. The correlation coefficient for the plotted data using this equation is R=0.76505. The relatively low value for the correlation coefficient is due to the limited number of tensile tests which have been performed on V-4Cr-4Ti.

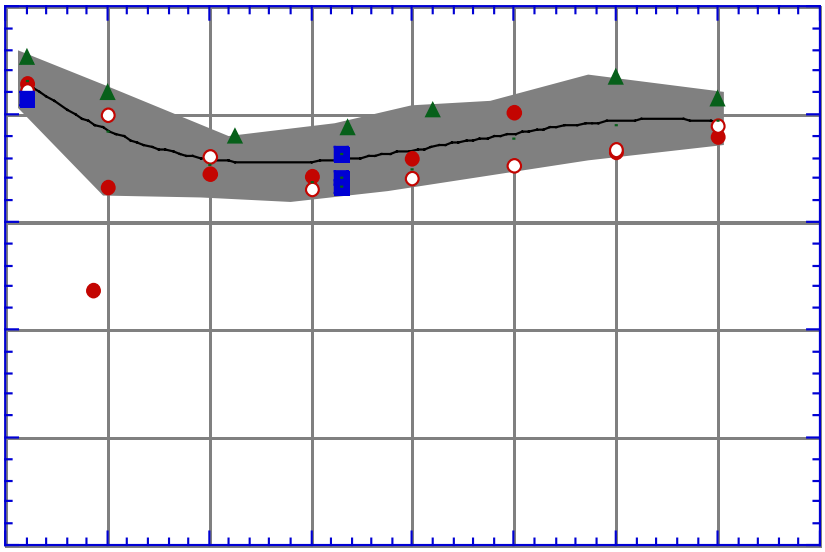

Fig. 3: Ultimate tensile strength of unirradiated V-4Cr-4Ti [1-3].

Fig. 4 summarizes the yield strength and uniform elongation data obtained in tensile tests at strain rates near $1x10^{-3}$ s^{-1} on annealed (1000-1100•C for 1 to 2 h) specimens in the longitudinal orientation for two different heats of V-4Cr-4Ti. The data in refs. [14,15] were obtained on "type SS3" miniature sheet tensile specimens with gage dimensions of 0.76 x 1.52 x 7.6 mm, whereas the data in ref. [16] was obtained on round tensile specimens with gage dimensions of 4 mm diam x 20 mm. Good agreement was obtained for both types of specimen geometries over the investigated temperature range. The least squares fitted equation for the yield strength over the temperature range of 20-700•C is

$$\sigma_Y(\text{MPa}) = 377.16 - 0.70384*T + 0.00089973*T^2 - 1.2279e\text{-}07*T^3 - 1.9824e\text{-}10*T^4$$

where the temperature (T) is in •C. The correlation coefficient for the plotted data using this equation is R=0.94608.

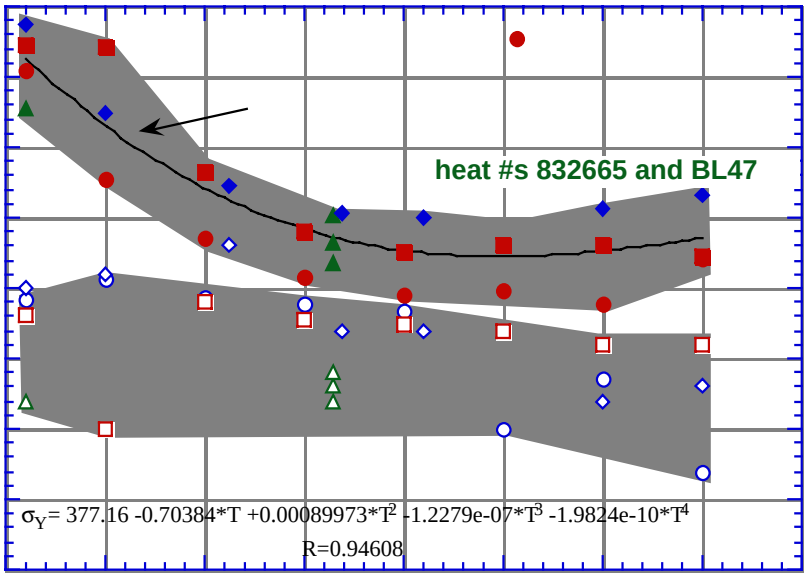

Fig. 4: Yield strength and uniform elongation of unirradiated V-4Cr-4Ti [1-3].

The elastic constants for V-5Cr-5Ti (heat BL63) have been measured at room temperature, and were found to be in good agreement with published data for pure vanadium [17]. The room temperature elastic constants were: Young's modulus E = 125.6±0.4 GPa, shear modulus G = 45.9±0.2 GPa, and Poisson's ratio 0.367±0.001. The following equations were recommended for extrapolation to temperatures above 20•C

$$E = ((1.28 - 9.61\times10^{-5} *T)\pm0.040) \times 10^{11} \text{ Pa, and}$$
$$G= ((0.488 - 8.43\times10^{-5} *T)\pm0.011) \times 10^{11} \text{ Pa.}$$

The thermophysical properties for V-5Cr-5Ti (heat BL63) have been measured from room temperature to 600•C, and are in agreement with published data for pure vanadium [18]. The instantaneous coefficient of thermal expansion varied from 9.1 ppm/•C at room temperature to 11.0 ppm/•C at 600•C. The fitted polynomial expressions for the linear thermal expansion ($\bullet L/L_0$) relative to the 20•C value and the instantaneous thermal expansion coefficient (α_{th}) are:

$$\bullet L/L_0 = -179.976 + 9.036385*T + 0.00154075* T^2 \quad \text{ppm}$$
$$\alpha_{th} = 9.03767 + 0.00301422*T + 4.95937\times10^{-7} * T^2 \quad \text{ppm/•C}$$

where the temperature (T) is given in •C. The thermal conductivity at 20-600•C was determined from thermal diffusivity measurements using either laser flash or xenon flash techniques with an overall accuracy of ±6%. The thermal conductivity was found to be in good agreement with literature values for pure vanadium. The least squares fitted equation for the thermal conductivity is

$$k_{th} = 27.827 + 0.008603\ T \quad W/m\text{-}K$$

where the temperature (T) is given in Kelvin.

Additional work on unirradiated and irradiated specimens is needed before the maximum and minimum operating temperature limits for vanadium alloys can be established. The following reference operating temperature limits of 400 and 700•C are proposed until these data become available. The reference minimum operating temperature limit will be controlled by radiation hardening, which causes loss of ductility and an increase in the ductile to brittle transition temperature. According to analyses of the DBTT in unirradiated and irradiated V-4Cr-4Ti specimens, brittle fracture behavior in MCVN specimens occurs when the yield stress exceeds ~700 MPa [19-21]. Based on the data, it is recommended that the irradiation temperature must be greater than ~400•C to avoid brittle fracture behavior in structures containing undetected cracks.

The maximum operating temperature limit will likely be controlled by either thermal creep (creep rupture), helium embrittlement or chemical compatibility/corrosion effects. Significant thermal creep is expected in V-4Cr-4Ti at or above ~700•C (0.45 T_M), but experimental creep data on this alloy [24] are only available at 600•C (0.4 T_M). Slow strain rate tests to check for helium embrittlement effects have not been performed on irradiated V-(4-5)%Cr-(4-5)%Ti alloys. Tensile tests performed on some other neutron-irradiated vanadium alloys containing fusion-relevant amounts of helium have generally not observed pronounced helium embrittlement at ≥700•C, but creep-rupture tests on helium-containing irradiated specimens are needed to further investigate this issue [25-28]. Whereas vanadium alloys have good compatibility with liquid lithium at temperatures up to 600•C, interstitial solute pickup and predicted corrosion rates become significant at 650-700•C [29-30]. These corrosion and interstitial solute pickup effects might be mitigated if fully adherent self-healing insulator coatings can be successfully developed.

C) SIC-SIC COMPOSITES

The engineering database for SiC/SiC composites is very limited, since large quantities of high-quality fibers such as Hi-Nicalon type S have not been available up to the present time. Much of the published data has been generated composites fabricated with lower-quality fibers such as ceramic grade Nicalon (cg-Nicalon). The chemical composition, density, elastic constants, thermal conductivity, and neutron radiation resistance of cg-Nicalon is considerably different from that of bulk crystalline SiC which is present in the matrix.

Most of the available data on ceramic matrix composites has been generated using flexural bend strength tests (3- or 4-point bending). Although bend tests are useful for qualitative screening in order to investigate variations in processing parameters, uniaxial tensile testing is preferred for the generation of an engineering data base. Ceramic matrix composites are

engineered to produce a moderate amount of fiber pullout during deformation. Extensive fiber pullout produces low ultimate tensile strengths, whereas limited fiber pullout leads to brittle failure modes similar to monolithic ceramics. The optimum tensile toughness generally occurs in composites with tensile elongations on the order of ~0.2 to 0.5%. Therefore, the 0.2% "yield" strength, which is commonly used for tensile testing in metals, is comparable to the ultimate tensile strength. A more appropriate "yield" strength for ceramic matrix composites is the proportional stress limit (corresponding to the onset of matrix microcracking), although the location of the proportional limit is subject to relatively large experimental uncertainty.

The ultimate tensile strength of several different grades of SiC/SiC composites (0/90 weave) have recently measured by tensile testing [31]. The UTS ranged from 200 to 240 MPa at room temperature and from 228 to 254 MPa at 1000•C for two different types of SiC/SiC composites fabricated with cg-Nicalon fibers. A room temperature UTS of 217 MPa was measured for a composite fabricated using Hi-Nicalon fibers. The corresponding proportional stress limits were 55 to 70 MPa for room temperature tests of SiC/SiC composites fabricated with cg-Nicalon fibers. Tensile data are not yet available for SiC/SiC composites fabricated with Hi-Nicalon type S fibers, although composite strengths comparable of slightly superior to that of present-day SiC/SiC composites are expected from theoretical considerations.

The elastic constants for SiC/SiC composites depend on the details of the fabrication procedure. Fibers such as cg-Nicalon have elastic constants which are considerably different from crystalline SiC, and therefore strongly influence the measured elastic constants of the composite. In addition, matrix porosity (typically ~8 to 10%) also affects the elastic constants of the composite. The room temperature Young's modulus of fibers ranges from 173 GPa for cg-Nicalon to 267 GPa for Hi-Nicalon and 403 GPa for Dow Sylramic [32]. The corresponding Young's modulus for bulk crystalline SiC varies from 460 GPa at room temperature to 435 GPa at 1000•C [33]. According to measurements obtained during tensile testing, the Young's modulus for a given SiC/SiC composite shows a very slight (5%) increase as the temperature is increased from 20 to 1000•C [31]. The quantitative values are strongly dependent on the fabrication process, with values for cg-Nicalon fiber-based composites ranging from 141 to 215 GPa at room temperature [31]. The corresponding Young's modulus for a SiC/SiC composite fabricated with Hi-Nicalon fibers was 270 GPa. Values approaching 400 GPa would be expected for high-quality, low-porosity SiC/SiC composites fabricated with Sylramic or Hi-Nicalon type S fibers.

The shear modulus for bulk SiC is ~165 GPa .
The Poisson's ratio for bulk SiC is 0.20 [33].

The themophysical properties of SiC/SiC composites (particularly thermal conductivity) are also dependent on the fabrication procedure. The measured instantaneous coefficient of thermal expansion (α_{th}) for SiC/SiC composites fabricated with cg-Nicalon fibers are 2.5-3 ppm/•C, with no apparent dependence on temperature between 20 and 1000•C [31]. The lower value refers to through-thickness measurements on 2-D composites, and the higher value refers to in-plane measurements. The bulk SiC value is 2.2 ppm/•C at room temperature and 5.0 ppm/•C at 1000•C, with an average value between 20 and 1000•C of 4.0 ppm/•C [33].

The thermal conductivity of SiC/SiC composites is strongly dependent on the processing conditions, type of fiber, and fiber architecture. The upper limit for thermal conductivity corresponds to that obtained in single crystal and high-purity CVD SiC, with maximum values of ~400 W/m-K at room temperature and 78 W/m-K at 1000•C (Fig. 5). The thermal conductivity of commercial fibers presently available is significantly lower than that of bulk high-purity SiC, and therefore they do not make a large contribution to the conductivity of the composite. The thermal conductivity of SiC-based fibers at 500•C varies from ~3-5 W/m-K for cg-Nicalon and ~5 W/m-K for Hi-Nicalon to 15 W/m-K for Hi-Nicalon type S [34]. The in-plane thermal conductivity for a 2-D (0/90) plain weave SiC/SiC composite fabricated from cg-Nicalon fibers (40 vol.%) and a CVI matrix (10% porosity) varies from ~19 W/m-K at 20•C to 8 W/m-K at 1000•C [31]. The corresponding through-thickness conductivities are 9 and 3 W/m-K, respectively. The through-thickness thermal conductivity for a 2-D (0/90) plain weave SiC/SiC composite fabricated from Hi-Nicalon fibers (40 vol.%) and a CVI matrix (10% porosity) is ~15 W/m-K at 20•C [31]. SiC/SiC composites with thermal conductivities of ~75 W/m-K at room temperature and 30-35 W/m-K at 1000•C have recently been fabricated using CVR and reaction sintering techniques [35,36].

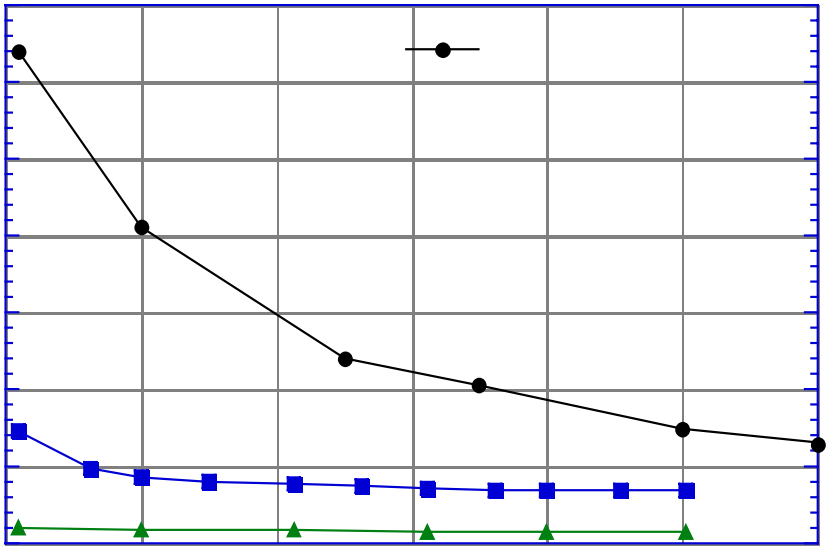

Fig. 5: Comparison of the thermal conductivity of monolithic CVD SiC and two grades of SiC/SiC composites.

The minimum operating temperature limit will be determined by either the crystalline to amorphous transition temperature (~120•C for fusion reactor damage rates) [37], or else radiation-induced degradation in the thermal conductivity. The thermal conductivity degradation becomes less pronounced with increasing irradiation temperature up to ~900•C, due to a decrease in the saturation concentration of point defect clusters. The maximum temperature

limit will likely be determined by void swelling considerations, although there are not sufficient data at elevated temperatures (900-1400•C) to make a clear determination. The tentative reference minimum and maximum operating temperature limits for the purposes of the APEX design study are 400•C (due to thermal conductivity degradation concerns) and 1000•C (due to void swelling concerns).

II.2 Refractory Alloys

Three high-temperature, refractory alloys are also considered here; Nb-1Zr, T111 and TZM. A summary of properties that is pertinent to the evaluation of the limits of these materials is presented here. TZM and Nb-1Zr have been previously considered for divertor designs.

A) TZM (Mo-0.5Ti-0.1Zr)

The properties included here are summarized from a document distributed by Plansee International, a producer and a vendor of refractory materials. Fig. 6 shows that ultimate and yielding tensile strengths of TZM as a function of temperature. The material, known as a heat resistant material, maintains its strength up to 1200•C or higher. Fig. 7 shows tha temperature dependence of Young's modulus of the alloy. Equations which fit the data are also shown. The coefficient of thermal expansion increases from 5ppm/•C at room temperature to 10 ppm/•C at 2000•C. The thermal conductivity decreases in a linear fashion from 130 w/mK at room temperature down to 75 w/mK at 2000•C. More data are avialable in Ref. [39]. The maximum operating temperature is considered here to be 1200•C based on thermal creep considerations.

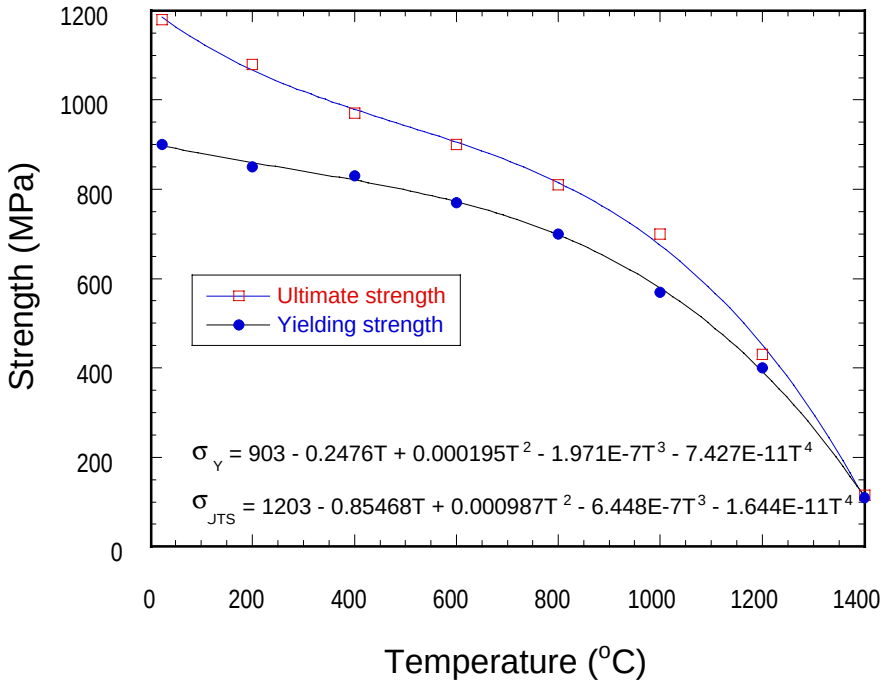

Fig. 6: Ultimate and yield tensile strength of TZM [38].

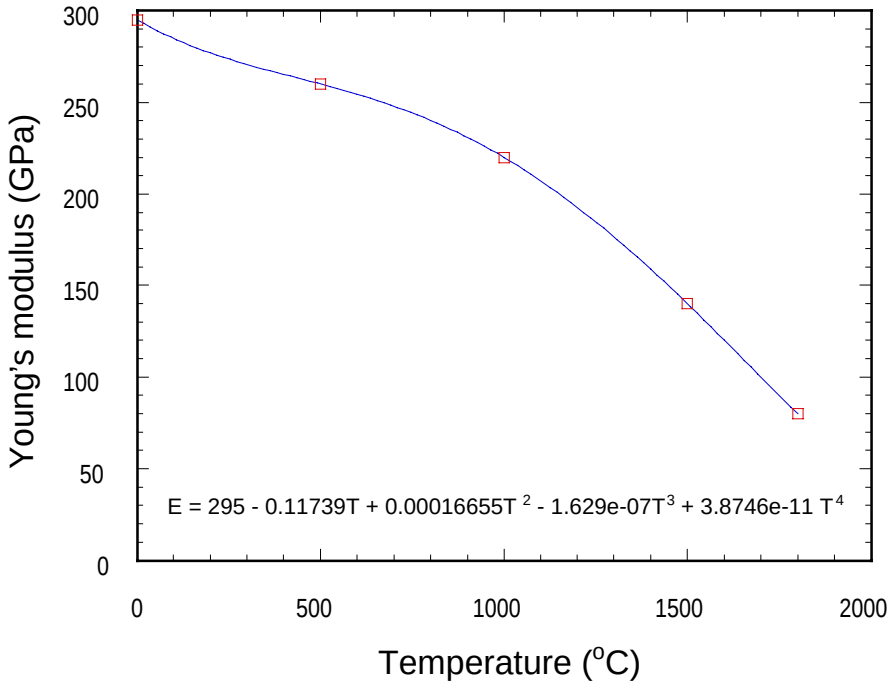

Fig. 7: Young's modulus of TZM [38].

B) Nb-1Zr

The ultimate and yielding tensile strength of Nb-1Zr are shown in Fig. 8 as a function of temperature [38]. The ultimate tensile strength data show a broad range of variation atthe same temperature and the data shown here are selected at the midlle of that range. As compared with TZM, Nb-1Zr is significantly softer. The elastic modulus is 104 GPa. The average value of the coefficient of thermal expansion is 7.2 ppm/•C in the range room temperature (RT) to 100•C, 7.88 ppm/•C in the range RT-1000•C, and 10 ppm/•C in the range RT to 1500•C. The thermal conductivity increases linearly from 52 w/mK at RT to 65 w/mK at 600•C. The recommended maximum operating temperature is about 1200•C based on thermal creep considerations.

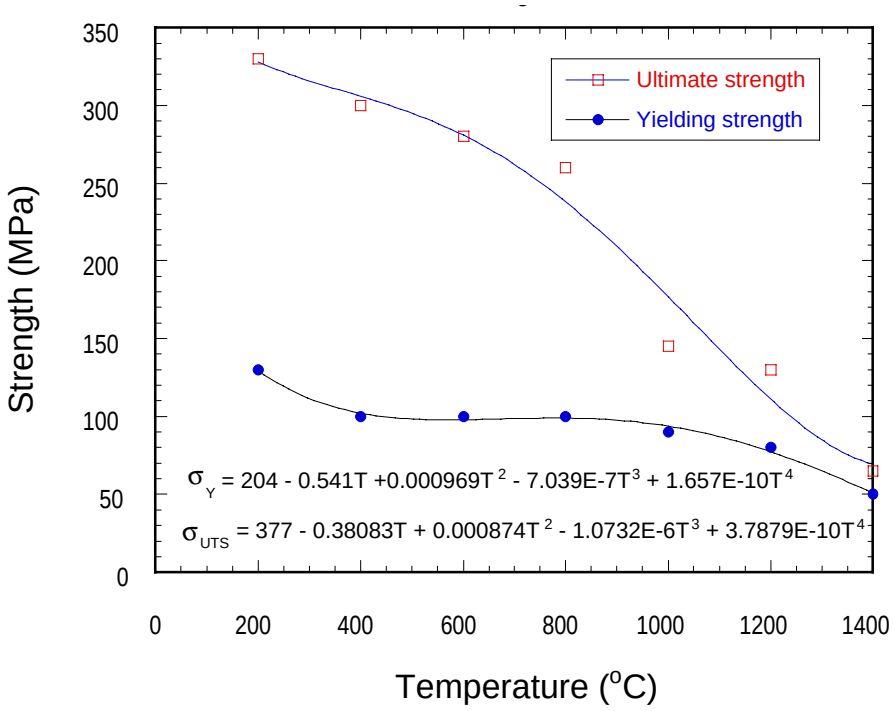

Fig. 8: Ultimate and yielding tensile strength of Nb-1Zr [38].

C) T111 (Ta-8W-2Hf)

The tesnile ultimate and yielding strength of T111 are shown in Fig. 9 and its Young's modulus is shown in Fig. 10 [39]. This alloy is much stronger that Nb-1Zr. The modulus of this alloy decreases fairly linearly with temperature from about 180 GPa at RT down to 130 GPa at 2000•C.The thermal conductivity increases from 42 w/mK at RT to 55 w/mK at 870 •C. The coefficient of thermal expansion increase from ~ 5ppm/K at RT to ~7.6 ppm/K at 1600 •C. The recommended maximum operating temperature is about 1500 •C; approximately half the melting point of the alloy.

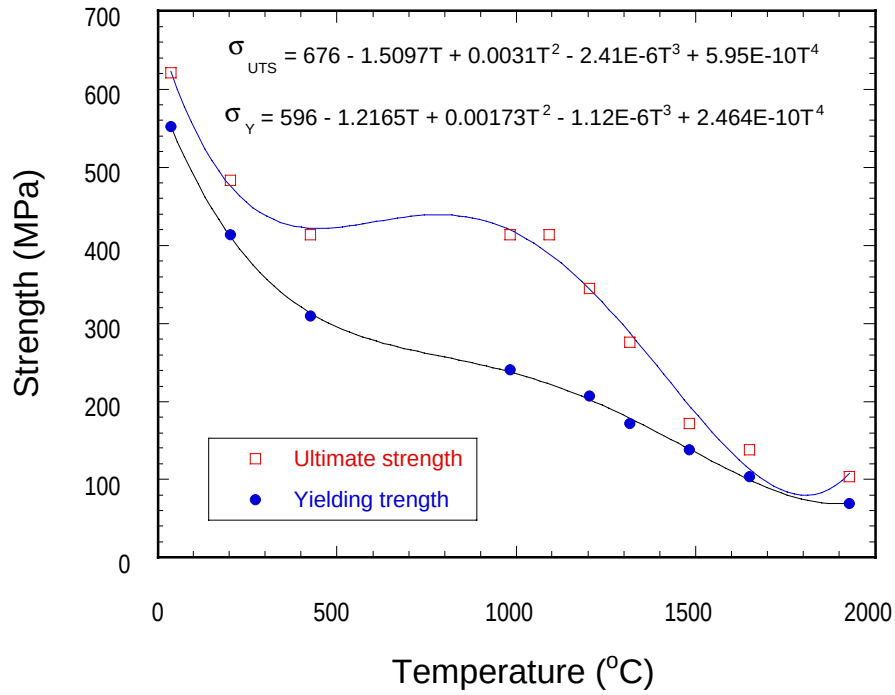

Fig. 9: Ultimate and yielding tensile strength of T111 [39].

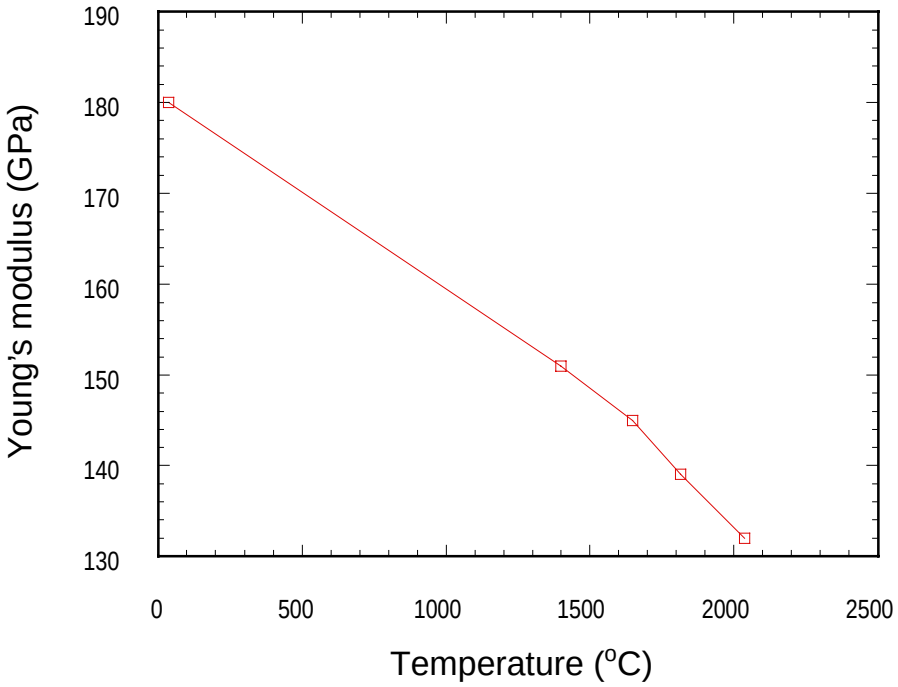

Fig. 10: Yougn's modulus of T111 [39].

III. FW CONFIGURATION & ASSUMPTIONS

The assumptions used in assessing the loading limits for conventional FWs made out of the materials discussed in the previous section are as follows:

- The solid first wall is modeled as a plate which is cooled from one side, and subjected to plasma radiation on the other side as well as nuclear bulk heating.
- The radiation heat flux is taken to be 0.2 Mw/m^2 per 1 Mw/m^2 neutron wall loading. The nuclear heating in the FW is assumed to be 10 w/cm^3 per $1Mw/m^2$ neutron wall loading. Typically, these values correspond to the average radiative heat flux (incident on the wall from the plasma side) and the average nuclear heating in the European Breeder-Out-of-Tube (BOT) Blanket Design.
- No peaking factors are considered.
- Stress limits for the metallic alloys are taken to be functions of the average wall temperature and no radiation effects (creep or swelling) are considered. Temperature-averaged values of other material properties are used in the calculations.
- The wall temperature profile is parabolic due to the combined bulk and surface heating. The thermal stress however is considered to be proportional to the temperature drop across the wall.
- A primary stress of 20MPa is considered, corresponding to hoop stress due to coolant pressure and other constraints. This is an approximation and the actual value of that stress may be different.
- The NWL limits are determined by comparing the total (thermal plus primary) stress to the $3S_m$, where S_m = min ($\sigma_{UTS}/3$, $2\sigma_Y/3$). This applies only to Ferritic steel and V-Cr-Ti alloys.
- In the case of SiC-SiC composites, the NWL limit is calculated by direct comparison of the induced stress to the material stress limit (either matrix cracking stress or the ultimate tensile stress).

The stress criterion used here to find the NWL limits for metallic alloys is a conventional criterion which is used by the “Fusion Community” to screen out and compare materials. For SiC-SiC composites, the story is different. In order for the calculations to make sense, one should invoke how the induced stresses cause the material to fail. For example, the addition of thermal stresses and primary stresses is incorrect, as these stresses lead to different failure paths/mechanisms. This statement is explained as below.

Primary stresses result from direct loading. These stresses are of the same nature as those applied during machine testing of materials samples. Therefore, if the induced stresses are mainly due to direct loading, i.e., primary, it may be permissible to compare these stresses with one of the measured material failure stress, even though this requires accounting for the material anisotropy in both deformation and failure should we speak of SiC-SiC. However, if the induced stress is mainly due to temperature gradients and/or constraining the structure while changing its temperature (even uniformly) the induced stresses lead to failure by mechanisms which are fundamentally different from those resulting during direct loading. In the simplest case of uniform changes in temperature of a (simple) structure made of composites with no constraints, microscopic stresses of large magnitude still develop due to the heterogeneous

nature of the material. Even though these stresses average to zero at the macroscopic level, they can still result in severe damage of the material.

A detailed study of the evolution of internal stresses in SiC-SiC composites under hi-temperature neutron irradiation was conducted [40]. A simplified geometrical model of a composite cylinder consisting of a single fiber embedded in the matrix was analyzed. Examples of the evolution of the internal stresses in the composite are given in Figs. 11 and 12. Initial mismatch stresses, differential swelling and thermal and irradiation creep rates were considered. The internal stresses are found to buildup by differential swelling and relaxed by creep. What is important to mention here is that significant changes in the bulk temperature may result in severe levels of internal stresses, even though with zero net macroscopic value. This has important implications in assessing the effects of induced thermal stresses in ceramic composites.

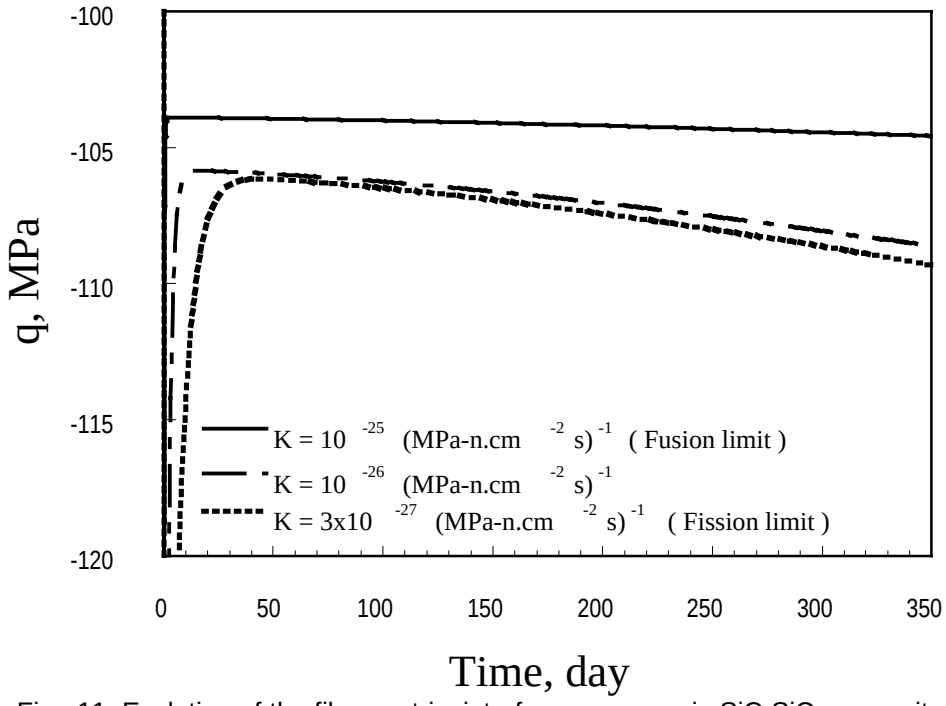

Fig. 11: Evolution of the fiber-matrix interface pressure in SiC-SiC composites in an ARIES-like environment [40]. K is the irradiation creep rate constant.

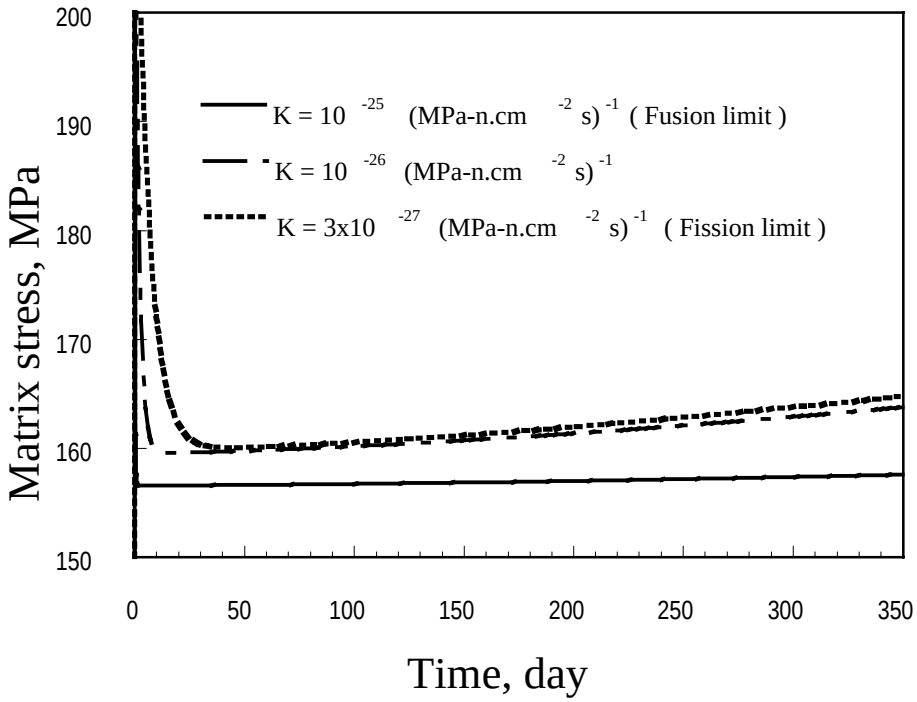

Fig. 12: Evolution of the tensile matrix stress in SiC-SiC composites in an ARIES-like environment [40]. K is the irradiation creep rate constant.

In violation of the discussion presented here, the induced thermal stresses are compared with the matrix cracking stress or the ultimate stress limits for SiC-SiC composites, and the results should looked at with these facts in mind.

IV. RESULTS AND DISCUSSION

II.1 Reduced-Activation Materials

It is clear from Figs. 13 through 19 that the neutron wall loading is limited by the materials stress and temperature limits for the three reduced activation materials, ferritic steel, vanadium-based alloys, and SiC-SiC composites. This of course represents a serious constraint on realizing high power densities. The materials limits are exceeded for moderate NWL, and this is mainly due to the fact that heat must be conducted through the first wall. A temperature drop must be established, thus thermal stresses build up. One way to avoid this problem is to utilize a mechanism of heat transfer which is not limited by heat conduction through the first wall in the conventional sense. A number of concepts are currently under evaluation where the direct loading of FW with radiation from the plasma is avoided or the transport of surface heat loads is enhanced by relying on other heat transfer mechanisms.

The 550 °C temperature limit for ferritic steel restricts the thermal efficiency since it will be exceeded for a coolant-structure interface temperature below 400 °C, which means that the exit coolant temperature is of the order of 350 °C. Similar exit temperatures from a V-Cr-Ti first wall are expected. Even though the creep/swelling temperature limit is about 650 °C for a V-Cr-

Ti first wall, the compatibility with hydrogen and oxygen environments start to be a limiting factor above 300-400 °C which poses more problems. For SiC based first wall, the mismatch stresses which are inherent to multi-phase materials such as SiC-SiC composites represent a serious issue, which is yet to be investigated. The material behavior is governed by a strongly heterogeneous micro structure. Unless the thermo-mechanical behavior of the two phases is similar, significant levels of internal stresses develop. These stresses are determined by: thermal expansion, swelling , creep rate , modulus mismatches. As mentioned previously, these stresses can lead to significant matrix cracking during heating or cooling with •T of few-several hundred degree, even if the macroscopic temperatures gradients are negligible. Stress levels of hundreds of MPa can be reached which is far beyond the matrix cracking levels. Matrix microcracking results in: changes in modulus and thermal conductivity, high coolant leakage rates, further material degradation (bulk of the material-fiber and fiber-matrix interface- is exposed to any chemical species present in the system), and structural problems.

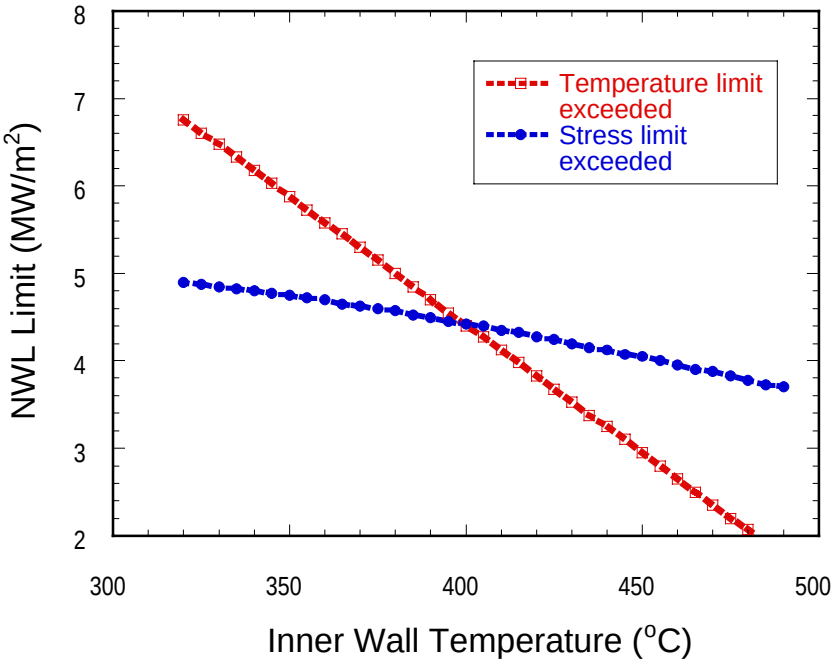

Fig. 13: NWL limit for a 5 mm thick Ferritic Steel FW.

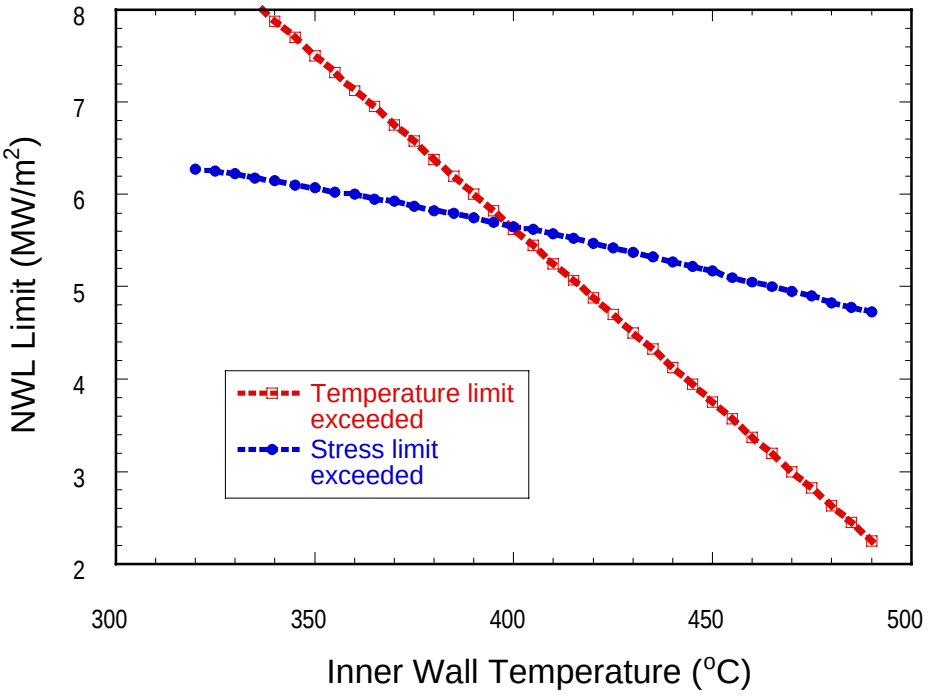

Fig. 14: NWL limit for a 4 mm thick Ferritic Steel FW.

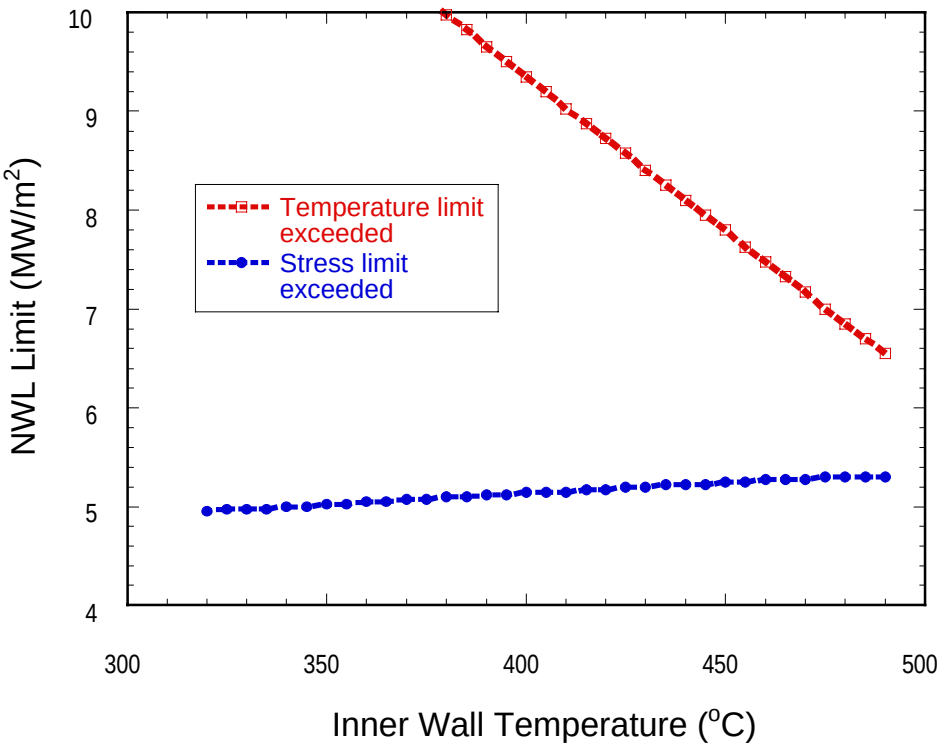

Fig. 15: NWL limit for a 5 mm thick V-Cr-Ti FW.

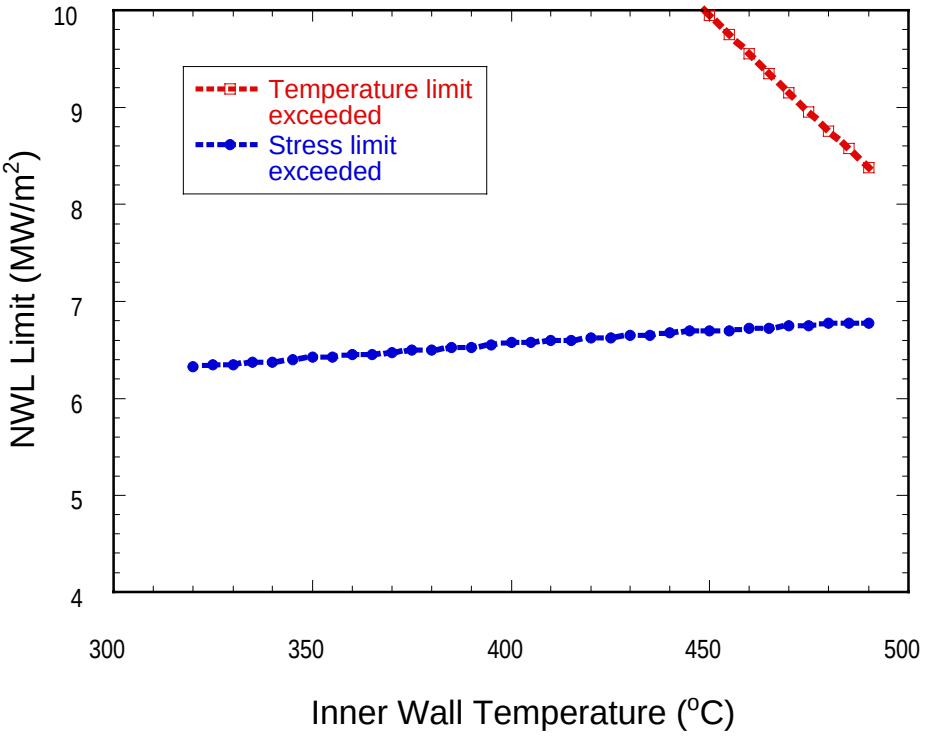

Fig. 16: NWL limit for a 4 mm thick V-Cr-Ti FW.

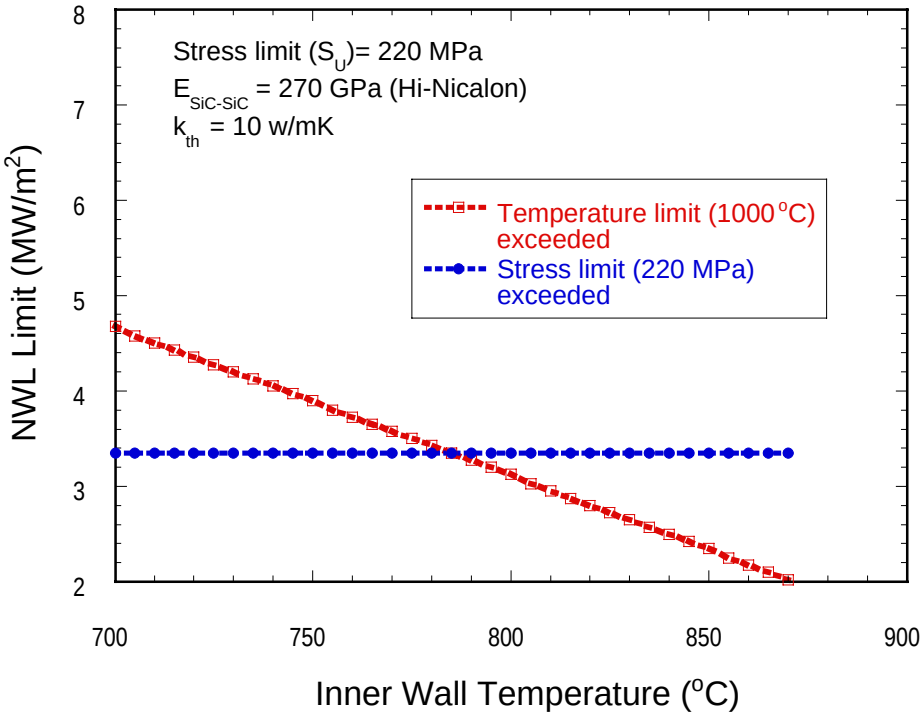

Fig. 17: NWL limit for a 3 mm thick SiC-SiC FW (conductivity = 10w/mK) . The NWL limit is proportional to the stress limit. If a lower stress limit is considered, the "stress limit curve" should be shifted down.

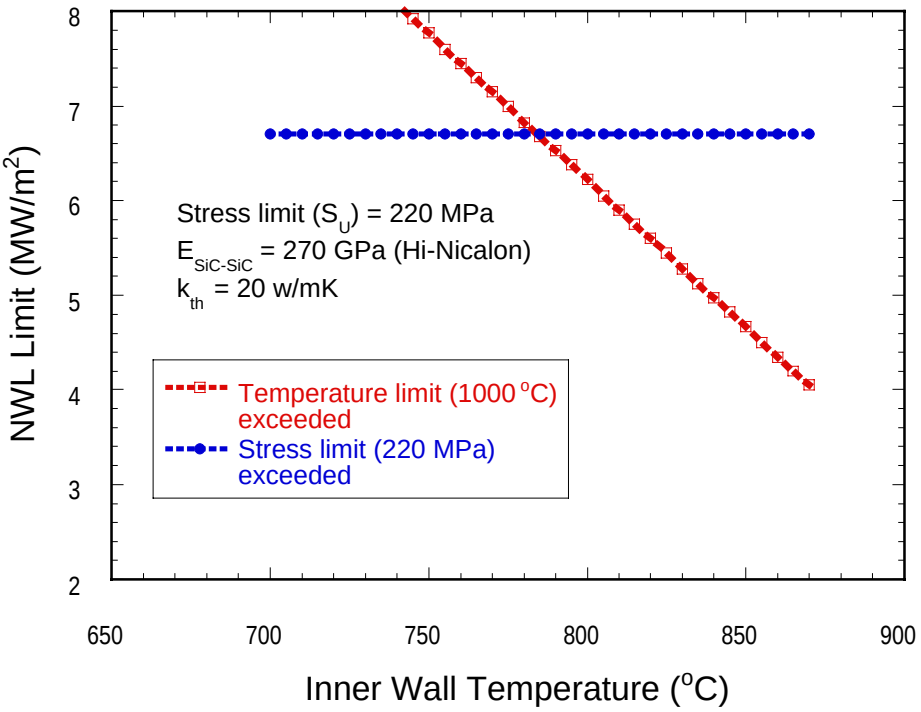

Fig. 18: NWL limit for a 3 mm thick SiC-SiC FW (conductivity = 20w/mK) . The NWL limit is proportional to the stress limit. If a lower stress limit is considered, the "stress limit curve" should be shifted down.

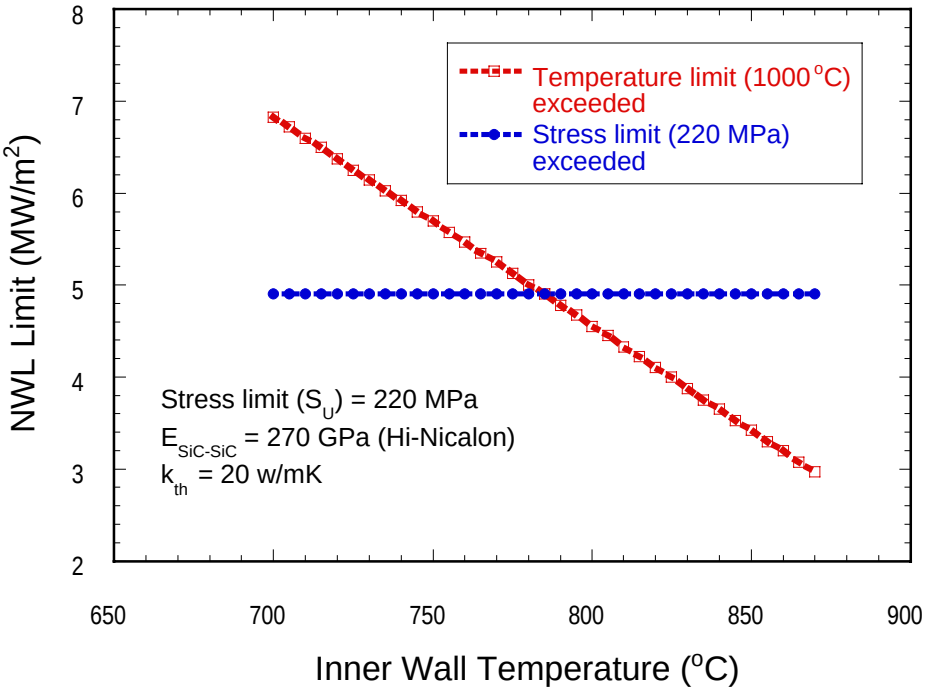

Fig. 19: NWL limit for a 4 mm thick SiC-SiC FW (conductivity = 20w/mK) . The NWL limit is proportional to the stress limit. If a lower stress limit is considered, the "stress limit curve" should be shifted down.

II.2 Refractory Alloys

Figs. 20 through 25 show the neutron wall load limits for the three alternate materials, TZM, T111 and Nb-1Zr. The NWL limits for Nb-1Zr are very similar to those for vanadium and steel. The reason is that this material exhibits inferior yielding and ultimate tensile strength characteristics, even though it can serve at much higher temperatures. TZM and T111 do not impose any constraints on NWL, and in principle, a nuclear power core with FW made of any of these two materials can withstand wall loads two or three times higher that ferretic steel or vanadium alloys.

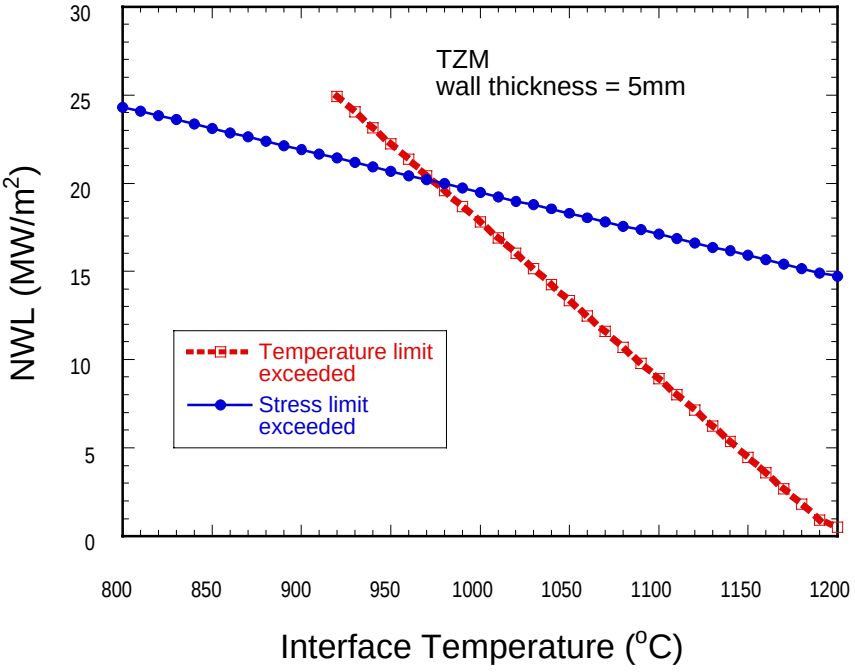

Fig. 20: NWL limit for a 5 mm thick TZM FW.

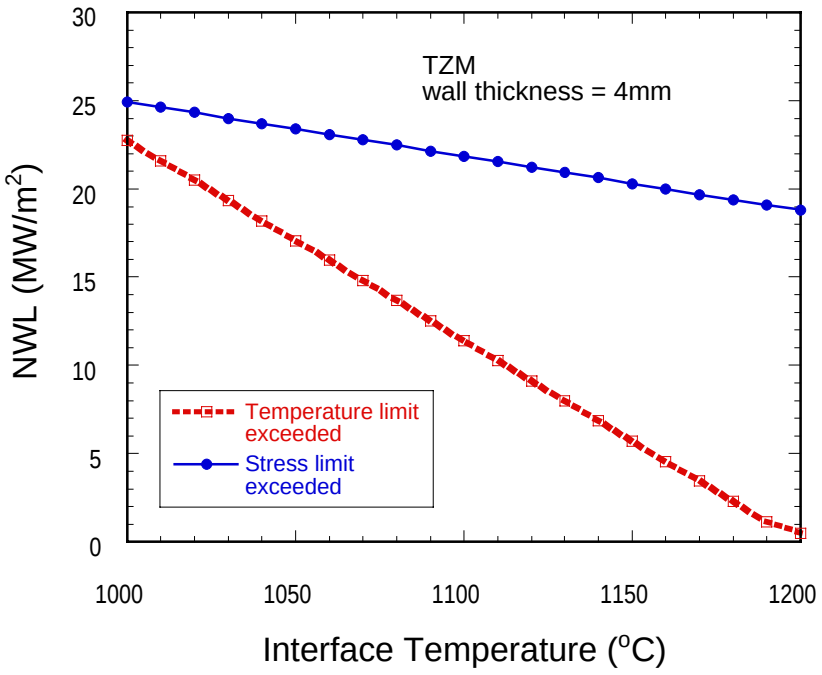

Fig. 21: NWL limit for a 4 mm thick TZM FW.

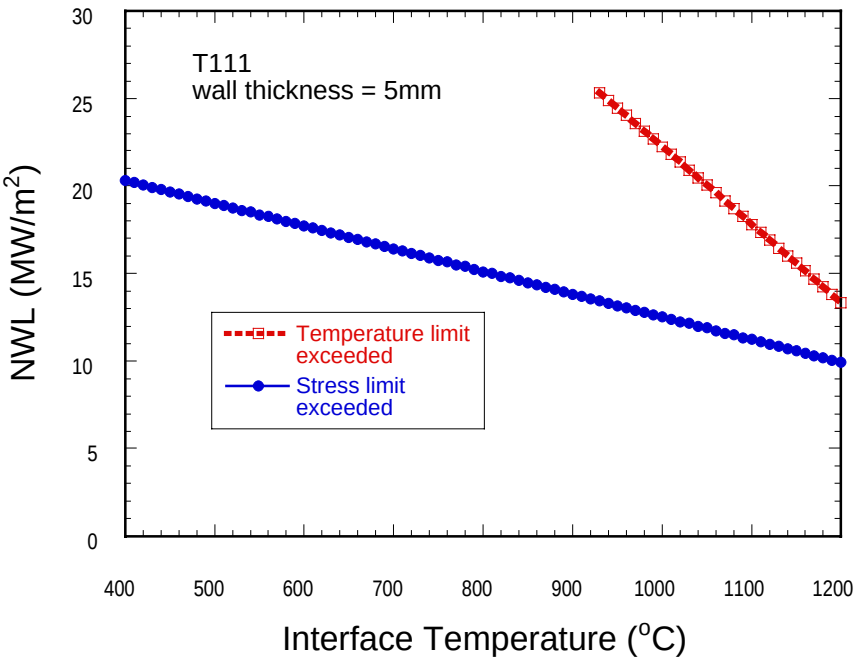

Fig. 22: NWL limit for a 5 mm thick T111 FW.

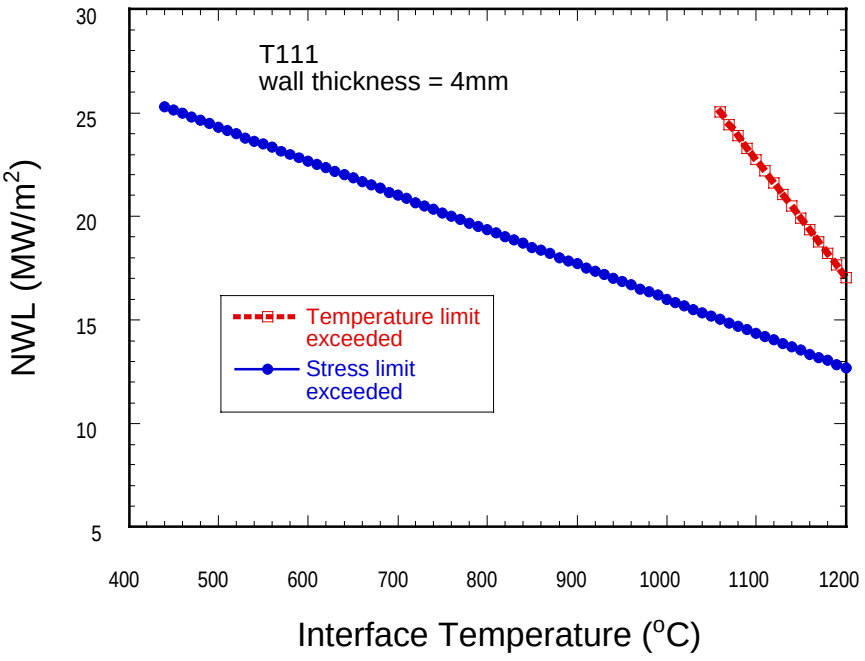

Fig. 23: NWL limit for a 4 mm thick T111 FW.

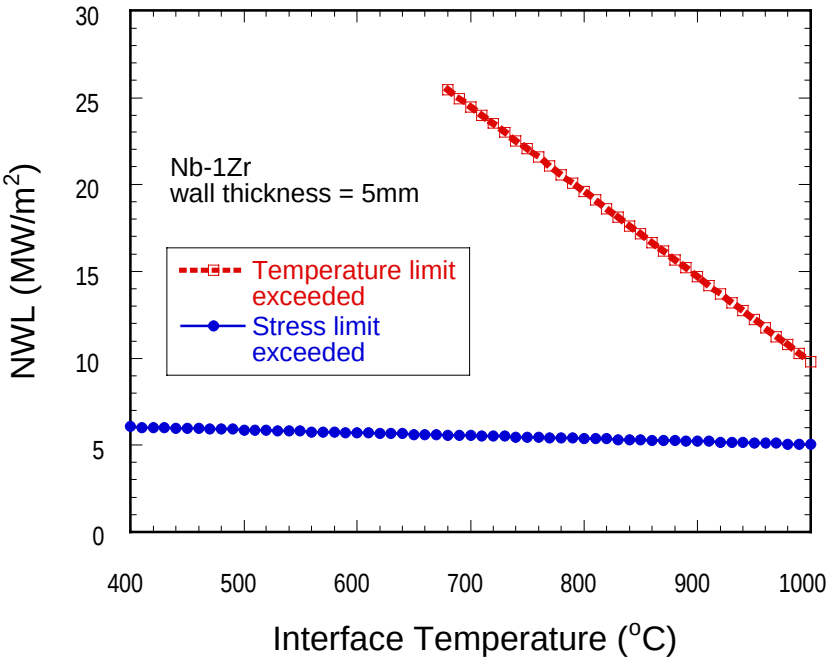

Fig. 24: NWL limit for a 5 mm thick Nb-1Zr FW.

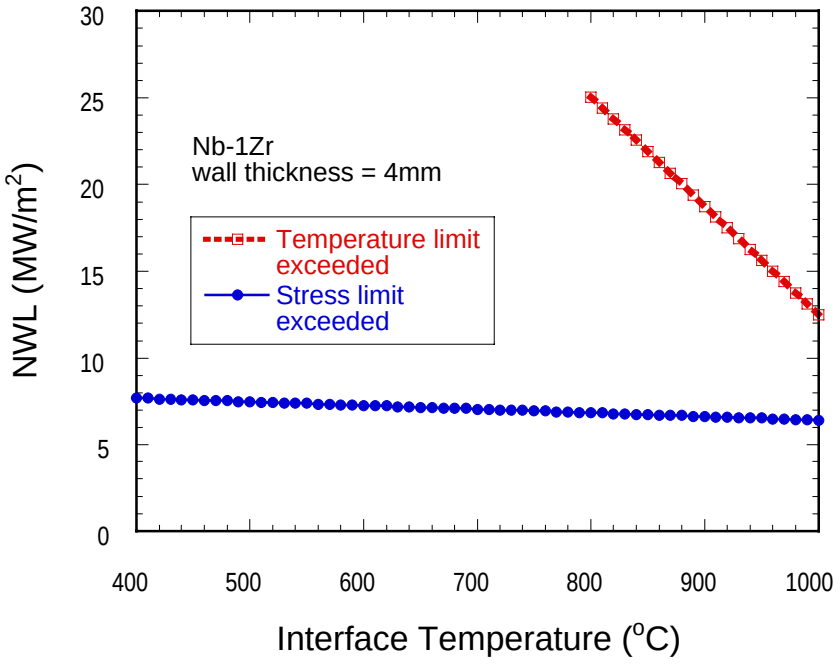

Fig. 25: NWL limit for a 4 mm thick Nb-1Zr FW.

V. CONCLUDING REMARKS

The present analysis has shown that materials property limits pose stringent constraints on the design window in current magnetic fusion device concepts. Specifically, the high power density capabilities of these concepts are significantly limited if the three reduced-activation materials are considered the only options. There is, therefore, a need to look into the possibility of using refractory materials and set aside the low activation requirements and/or search for highly innovative concepts which utilize the present three low activation candidate materials. The main objectives of the APEX study are indeed defined to be in this direction.

REFERENCES

[1] Recent experimental data from JET.
[2] N. Yamamouchi et al., J. Nucl. Mater. 191-194 (1992) 822.
[3] K. Ehrlich, in: R.L. Klueh (Ed.) Proc. IEA Working Group Meeting on Ferritic/Martensitic Steels, Culham, UK, October 1996, ORNL/M-5674, Oak Ridge National Lab, 1996.
[4] K. Shiba, N. Yamanouchi, A. Kohyama, Fusion Materials Semiannual Progress Report for Period ending June 30, 1996, DOE/ER-0313/20, Oak Ridge National Lab, 1996, p. 190.
[5] J.P. Robertson et al., presented at 8th Int. Conf. on Fusion Reactor Materials, Sendai, (1997) to be publ. in Fusion Materials semiann. Prog Rep. for period ending Dec. 31 1997.
[6] R.L. Klueh, D.J. Alexander, J. Nucl. Mater. 187 (1992) 60.
[7] R.L. Klueh, D.J. Alexander, J. Nucl. Mater. 230 (1996) 191.
[8] A.F. Rowcliffe et al., 8th Int. Conf. on Fusion Reactor Materials, Sendai, J. Nucl. Mater. (1997) submitted.

[9] A. Kohyama et al., Proc. ISFNT-4, Tokyo, Japan, , 1997, in press.
[10] G.E. Lucas et al., Fusion Materials Semiannual Progress Report for Period ending March 31, 1995, DOE/ER-0313/18, Oak Ridge National Lab, 1995, p. 147.
[11] A. Kohyama, in: R.L. Klueh (Ed.) Proc. IEA Working Group Meeting on Ferritic/Martensitic Steels, Culham, UK, October 1996, ORNL/M-5674, Oak Ridge National Lab, 1996.
[12] R.L. Klueh, D.J. Alexander, J. Nucl. Mater. 218 (1995) 151.
[13] L.E. Schubert, M.L. Hamilton, D.S. Gelles, Fusion Materials Semiannual Progress Report for Period ending June 30, 1996, DOE/ER-0313/20, Oak Ridge National Lab, 1996, p. 171.
[14] M.C. Billone, 8th Int. Conf. on Fusion Reactor Materials, Sendai, J. Nucl. Mater. (1997) submitted.
[15] A.N. Gubbi, A.F. Rowcliffe, W.S. Eatherly, L.T. Gibson, Fusion Materials Semiannual Progress Report for Period ending June 30, 1996, DOE/ER-0313/20, Oak Ridge National Lab, 1996, p. 38.
[16] E.V. van Osch, 8th Int. Conf. on Fusion Reactor Materials, Sendai, J. Nucl. Mater. (1997) submitted.
[17] W.A. Simpson, Fusion Materials Semiannual Progress Report for Period ending March 31, 1994, DOE/ER-0313/16, Oak Ridge National Lab, 1994, p. 258.
[18] W.D. Porter, R.B. Dinwiddie, M.L. Grossbeck, Fusion Materials Semiann. Prog. Report for Period ending March 31, 1994, DOE/ER-0313/16, Oak Ridge National Lab, 1994, p. 260.
[19] G.R. Odette, E. Donahue, G.E. Lucas, J.W. Sheckherd, Fusion Materials Semiann. Prog. Report for Period ending June 30, 1996, DOE/ER-0313/20, Oak Ridge National Lab, 1996, p. 11.
[20] D.J. Alexander et al., 18th ASTM Symp. on Effects of Radiation on Materials, Hyannis, MA, 1996, in press; also Fusion Materials Semiannual Progress Report for Period ending June 30, 1996, DOE/ER-0313/20, Oak Ridge National Lab, 1996, p. 87.
[21] G.R. Odette et al., 8th Int. Conf. on Fusion Reactor Materials, Sendai, J. Nucl. Mater. (1997) submitted.
[23] S.J. Zinkle et al., 8th Int. Conf. on Fusion Reactor Materials, Sendai, J. Nucl. Mater. (1997) submitted.
[24] H.M. Chung, B.A. Loomis, D.L. Smith, J. Nucl. Mater. 212-215 (1994) 772.
[25] W. van Witzenburg, E. deVries, in: R.E. Stoller, A.S. Kumar, D.S. Gelles (Eds.), 15th Int. Symp. on Effects of Radiation on Materials, ASTM STP 1125, American Society for Testing and Materials, Philadelphia, 1992, p. 915.
[26] B. Van Der Schaaf, J. Nucl. Mater. 155-157 (1988) 156.
[27] H. Matsui et al., in: A.S. Kumar et al. (Eds.), 16th Int. Symp. on Effects of Radiation on Materials, ASTM STP 1175, American Society for Testing and Materials, Philadelphia, 1993, p. 1215.
[28] A.I. Ryazanov, V.M. Manichev, W. van Witzenburg, J. Nucl. Mater. 227 (1996) 304.
[29] D.L. Smith, B.A. Loomis, D.R. Diercks, J. Nucl. Mater. 135 (1985) 125.
[30] V.A. Evtikhin, I.E. Lyublinski, V.Y. Pankratov, J. Nucl. Mater. 191-194 (1992) 924.
[31] E. Lara-Curzio, in: M.N. Rahaman (Ed.) Encyclopedia of Ceramic Engineering, Marcel Dekker, New York, 1998, p. in press.
[32] M.C. Osborne, C.R. Hubbard, L.L. Snead, D. Steiner, J. Nucl. Mater., Am. Ceram. Soc. Symp. on Fabrication and Properties of Ceramics for Fusion Energy and Other High Radiation Environments (1998) in press.
[33] Morton Advanced Materials product literature, Woburn, MA, 1995.

[34] K. Okamura, M. Narisawa, T. Yamamura, M. Sato, 8th Int. Conf. on Fusion Reactor Materials, Sendai, J. Nucl. Mater. (1998) submitted.
[35] A. Sayano et al., 8th Int. Conf. on Fusion Reactor Materials, Sendai, J. Nucl. Mater. (1998) submitted.
[36] W. Kowbel, (thermal conductivity of CVR silicon carbide matrix composites), 1997.
[37] L.L. Snead, S.J. Zinkle, J.C. Hay, M.C. Osborne, Nucl. Instr. Meth. B (1998) in press.
[38] Plansee International, Molybdenum, Metallwerk Plansee GmbH, 530 DEF 9.86.
[39] Aerospace Structural Metals Handbook, 1992 Edition, Vol. 5.
[40] A. El-Azab and N.M. Ghoniem, Viscoelastic Analysis of Mismatch Stresses in Ceramic Matrix Composites under High-Temperature Neutron Irradiation, Mechanics of Materials, 20 (1995) 291.